Oscillatory behavior of nanodroplets

S. Arcidiacono and D. Poulikakos*
Laboratory of Thermodynamics in Emerging Technologies, Swiss Federal Institute of Technology, ETH Zentrum, Sonneggstrasse 3, CH-8092 Zurich, Switzerland

Y. Ventikos
Department of Engineering Science, University of Oxford, Parks Road, Oxford OX1 3PJ, United Kingdom
(Received 13 February 2004; published 29 July 2004)

Molecular dynamics (MD) simulations were performed in order to investigate the phenomenon of free oscillations of nanodroplets and the extent to which the continuum theory for such oscillations holds at nanoscales. The effect of temperature on these oscillations is also studied. The surface tension, a key property for the phenomenon of interest, was evaluated and compared with the experimental values of argon, showing that with an appropriate choice of the cutoff distance in the MD simulations, it is possible to predict the surface tension with good approximation. Nanoscale capillary waves on the free surface of the droplet were observed and compared to continuum theoretical predictions of the same. The nanodroplet interface thickness calculated based on continuum theory for these waves agreed well with the molecular dynamics calculation of the interface thickness. The frequencies of the oscillation of the droplet were calculated for all the studied temperatures and compared with the classical continuum theory. Although the simulated system cannot be considered strictly as a continuum, a good overall agreement was found.

DOI: 10.1103/PhysRevE.70.011505 PACS number(s): 83.10.Mj, 83.50.−v, 68.05.−n

I. INTRODUCTION

The problem of oscillating liquid drops is relevant to several scientific fields and practical applications, such as cloud physics, containerless processing in low gravity, collision, coalescence, and break up of droplets in sprays, chemical processes, and measurement techniques of interfacial properties.

There is a rich literature on this subject for droplets described by continuum theory in all theoretical, numerical, and experimental domains. We report briefly select key results directly relevant to the present work.

Lord Rayleigh [1] investigated mathematically the nature of oscillations of an inviscid liquid drop and assuming small deformations. Neglecting the effect of the surrounding gas, the natural frequency of a free droplet of radius R, surface tension γ, and liquid density ρ_l, can be evaluated by

$$\omega_n^2 = \frac{\gamma}{\rho_l R^3} n(n-1)(n+2). \tag{1}$$

The fundamental oscillation mode in Eq. (1) is corresponding to $n=2$ whereas $n=1$ relates to a rigid spheroid. Subsequently, Lamb [2] studied the effect of small viscosity, i.e., $\mathrm{Re}=1/\nu(R\gamma/\rho)^{1/2}\gg 1$, where Re is the Reynolds number. With this hypothesis the frequency of the oscillation is the same as in Eq. (1) while the amplitude is damped exponentially as follows:

$$A = A_0 e^{-b_n t} \tag{2}$$

where A is the amplitude of the droplet oscillation, A_0 is the same quantity, but in the inviscid limit, t is the dimensional time, and b_n is the damping coefficient defined as follows:

$$b_n = (n-1)(2n+1)\nu/R^2. \tag{3}$$

The latter is a constant not depending on the restoring force, but only on the size of the droplet and its viscosity ν. Chandrasekhar [3] later obtained more general results for a viscous spheroid. Prosperetti [4] presented a theory for a viscous drop under infinitesimal amplitude oscillations. This analysis predicts that the system behaves as a damped oscillator which, when viscous effects are small compared with the inertial ones, is characterized by a natural frequency $(\omega_n^2-b_n^2)^{1/2}$. The analysis predicted also a transition from a periodic to an aperiodic decay as the viscosity increases, while for certain ranges of the parameter $1/\mathrm{Re}$, it is also possible to have an aperiodic oscillation that evolves into periodic.

Nonlinear effects due to moderate amplitude oscillations of an inviscid droplet were considered by Tsamopoulos (TS) and Brown [5] extending Rayleigh's analysis to second order for certain combinations of mode coupling. Their analysis predicted for the second oscillation mode a shift of the oscillation frequency with the increasing of the square of the initial amplitude of the oscillation A:

$$\omega_2' = \omega_2[1 - 0.63876A^2 + O(A^4)]. \tag{4}$$

Becker, Hiller, and Kowalewski [6] studied, both theoretically and experimentally, the oscillations of a free droplet generated from a break up of a liquid jet. They found that the frequency shift decreases with the square of the oscillation amplitude as predicted in [5], but with a larger rate and with

*Corresponding author.
Email address: dimos.poulikakos@ethz.ch

variations for different generated droplets depending on the initial internal flow field inside the drop.

The study of a realistic configuration, including nonlinearities of viscosity and large oscillations, requires solving the Navier-Stokes equations numerically. Basaran [7] performed a rigorous numerical study using a Galerkin/finite element technique for large oscillations of viscous drops and focusing on the oscillation of a drop released from the second spherical harmonic shape. The calculations showed a good agreement with the predictions of Prosperetti and TS analysis within their application limits. The influence on the oscillation period and decay factor due to initial internal circulations was investigated numerically by Mashayek and Ashgriz [8] showing that it can result in a significant change in the characteristics of the drop oscillation. Recently Pozrikidis [9] implemented a numerical method using a 3D generalized vortex formulation. The accuracy of the results obtained was dependent on the dominant droplet oscillation mode but was satisfactory overall.

On the experimental side, Trinh and Wang [10] studied the large amplitude oscillations of quasineutrally buoyant silicon oil and carbon tetrachloride levitated in distilled water. They found that the frequency decreases with increasing the square of the oscillation amplitude and, in an oscillation period, the prolate phase lasts longer than the oblate phase, confirming the predictions of Tsamopoulos and Brown [5]. A study of the oscillation of a low-viscosity droplet in a microgravity environment of a space shuttle flight was performed by Wang *et al.* [11]. The resulting frequency shift for the second-mode oscillation was in agreement with the predictions of the theory [5] for $A<0.3$. Azuma and Yoshihara [12] employed electrical excitation to obtain 3D, large amplitude oscillations of a mercury drop. A relationship between drop oscillation modes and frequencies was found. Nonlinear interaction of waves resulted in polyhedral oscillations.

The goal of the present work is to extend the previous findings for the second oscillation mode to nanoscales through the use of molecular dynamics (MD), investigating whether the applicability of the continuous theories is still valid for atomic clusters. Another important issue is that the MD simulations are 3D, thereby providing a complete view of the phenomena. In Sec. II the numerical method is described. Section III reports the results for the liquid-vapor interface, surface tension, and droplet oscillation. Conclusions are presented in Sec. IV.

II. MD SIMULATIONS

The studied argon nanodroplet consists of about 330 000 atoms interacting with the 12-6 Lennard-Jones pair potential

$$\Phi(r) = 4\varepsilon\left[\left(\frac{\sigma}{r}\right)^{12} - \left(\frac{\sigma}{r}\right)^{6}\right]. \tag{5}$$

The values for the parameters in Eq. (5) were chosen so as to mimic the gas argon ($\sigma=3.405$ Å and $\varepsilon=1.67\cdot10^{-21}$ *J*). The simulation domain is a cubic box of side $L=154.8\sigma$ with periodic boundary conditions in all the three directions.

The value of the cutoff distance is set to 4σ. This particular choice was suggested by the results of Trokhymchuk and Alejandre [13] who compared previous findings with their calculations for the surface tension evaluation of a planar film via MD and Monte Carlo simulations. They showed that differences found by diverse authors in surface tension evaluation were due to the potential used, shifted or nonshifted, and mainly to the assumed cutoff radius. They concluded that different methods are giving the same results for a cutoff distance larger than 4.4σ. A further comparison with experimental argon data [14] showed that a cutoff distance of approximately 4σ could reproduce the experimental data for argon, including the values of surface tension. The results are expressed in dimensionless form using the standard reference scales for a Lennard-Jones fluid (σ as length scale, ε as energy scale, and $\sigma\sqrt{m/\varepsilon}$ as time scale, where m is the mass).

We focus our attention on three different temperatures in this study: $T(\varepsilon/k_B)=0.81$, 0.9, and 0.97. The target temperature is reached by rescaling the particle velocities [15] every 250 time steps. The system is equilibrated until the average temperature is constant (this required up to 750 000 time steps for the case of $T(\varepsilon/k_B)=0.97$). The leap-frog algorithm is used to integrate the equation of motion with a dimensionless time step of 0.005 during the equilibration. The time step is halved during the droplet deformation-oscillation transient. Each calculation required one–two months using a parallel algorithm that employs simple spatial domain decomposition [16] on a 4 CPU DEC parallel machine.

III. RESULTS

A. Liquid-vapor interface

In nanoscopic droplets one must define a radius because the liquid-vapor interface is not sharply identified. It is common to characterize the droplet size with the equimolar dividing radius R_e as follows:

$$N = \rho_l\frac{4\pi}{3}R_e^3 + \rho_v\left(L^3 - \frac{4\pi}{3}R_e^3\right) \tag{6}$$

where N is the total number of atoms, ρ_l and ρ_v are, respectively, the liquid and vapor densities. The nonuniformity of the liquid-vapor interface is evident from observing the radial density profile in Fig. 1 for all the studied cases. The value of the density is constant within the liquid and the vapor regions, while the interface region is characterized by a thin layer where the density profile is decreasing monotonically from the liquid to the vapor value. The reported curves in Fig. 1 are relative to the equimolar dividing radius, so that the three curves are intercepting in the same point at $R=R_e$. The two asymptotic values of the density ρ_l inside the liquid and ρ_v inside the vapor can be obtained by fitting the density profiles with the formula:

$$\rho(r) = \frac{1}{2}(\rho_l+\rho_v) - \frac{1}{2}(\rho_l-\rho_v)\mathrm{erf}\left[\sqrt{\pi}\frac{(r-R_0)}{D}\right] \tag{7}$$

where D is a measure of the liquid-vapor interface thickness, R_0 is another path to estimate the droplet radius, defined as the radius at which the corresponding density is the average of the liquid-vapor asymptotic values. Numerically, R_0 is close to the quantity R_e defined in Eq. (6) (for the present

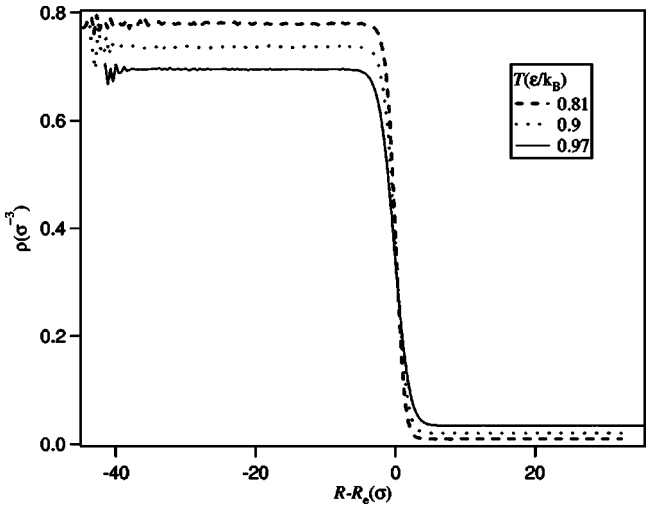

FIG. 1. Density profiles relative to the equimolar dividing radius for the three different studied temperatures.

calculations the discrepancy is less than 1%). The two parameters D and R_0 can also be obtained by fitting the density profile. The choice to fit the density profiles with the error function [Eq. (7)] rather than the usual hyperbolic tangent is supported by calculations of Sides, Grest, and Lacasse [17] stating a better prediction of the interface thickness, as well as by the work of Toxvaerd and Stecki [18]. Herein it is verified that the error in the fit of the density profile is smaller by around 10% compared to the fit performed with the hyperbolic tangent function. The prediction of interface thickness with the error function fit is by 5% larger compared to the hyperbolic tangent fit.

The thickness of the interface can be mostly explained by the presence of capillary waves excited by thermal energy. Capillary waves are nothing more than an expression of the internal Brownian motion that is randomly deforming the spherical shape of the droplet. This phenomenon is more evident in nanodroplets, because the amplitude of capillary waves is of the same order as the droplet radius. The thickness of the interface due to capillary waves can be evaluated analytically as a function of the mean-square displacement $\langle \zeta_{cw}^2 \rangle$ of the radius. A simplified theory for estimating $\langle \zeta_{cw}^2 \rangle$ was proposed by Bartell [19]. He found that the mean square displacement from the mean radius due to capillary waves of modes of energy $k_B T$, assuming it follows a Gaussian distribution, can be expressed as follows:

$$\langle \zeta_{cw}^2 \rangle = \sum_l \sum_m (k_B T / 2\pi\gamma I_{lm}) \tag{8}$$

where K_B is the Boltzmann constant, I_{lm} is the integral over the surface harmonics (a detailed formulation can be found in [19,20]), $m=l-2n$ (n is an integer including zero), and $l=2,3,\ldots,l_{\max}$. An estimation of $l_{\max}$ is obtained from the number of molecules in the periphery of a spherical cluster $N_c \cong 2\pi[(3N/4\pi)^{1/3}-1/2]$ and can be assumed of the order of magnitude of $N_c/2$. Equation (8) shows that the mean displacement is larger at higher temperatures. Finally the thickness of the interface can be expressed as [19]

TABLE I. Interface thickness due to capillary waves (D_{cw}) and calculated via MD (D). The last two lines are the temperature oscillation period t_T and the damping constant τ during the compression transient obtained by fitting the temperature profiles with Eq. (14) for all the studied cases.

$T(\varepsilon/k_B)$	0.81	0.9	0.97
$D_{cw}(\sigma)$: Capillary waves theory, Eq. (9)	2.23	2.70	3.39
$D(\sigma)$: MD, Eq. (7)	2.87	3.34	4.38
Temperature oscillation period $t_T(\sigma\sqrt{m/\varepsilon})$	18.4	20	21.4
Temperature damping constant $\tau(\sigma\sqrt{m/\varepsilon})$	88.5	74.8	61.3

$$D_{cw} = \langle 2\pi\zeta^2 \rangle^{1/2}. \tag{9}$$

Table I reports the values for D obtained via MD with Eq. (7) and the analytical formulation with Eq. (9). The ratio between the thicknesses D evaluated analytically and via MD is around 0.77 for the three cases considered. A similar result (value of 0.83) is reported by Bartell [19], where the prediction of Eq. (9) was compared with other previously performed MD simulations of smaller droplets [21,22] (the hyperbolic tangent function was used to fir the density profiles in these references). The fact that the above-mentioned ratio is smaller than unity is known [23]. There are two contributions to the liquid-vapor interface thickness: an intrinsic contribution due to the atomic structure of the fluid and a contribution of the thermally excited capillary waves that become more important with increasing the total surface area. The total mean square displacement can be written as the sum of the intrinsic and capillary wave contribution:

$$\langle \zeta^2 \rangle = \langle \zeta_i^2 \rangle + \langle \zeta_{cw}^2 \rangle \tag{10}$$

and it can be calculated defining it as the variance of the derivative of the density profile (7), leading to the expression [17]:

$$\langle \zeta^2 \rangle = D^2 / 2\pi. \tag{11}$$

A comparison with the experimental predictions for the planar interface thickness D and D_{cw} for argon [24] is reported in Fig. 2 as a function of $1-T/T_c$ where T_c is the critical temperature, showing good agreement. Discrepancies in D_{cw} are probably due to the different choice of the upper surface wave cutoff.

B. Surface tension

The surface tension of a droplet can be evaluated using the well-known Laplace formula:

$$\gamma = \frac{\Delta p \cdot R}{2} \tag{12}$$

where Δp is the difference between the pressure in the liquid p_l and the pressure in the vapor p_v phase, and R is the radius of the droplet. In the present work, it will be assumed that the cluster is large enough to neglect the curvature effects and we will consider in Eq. (12) $R=R_e$. This assumption is supported by the recent MD simulations of Bardouni *et al.*

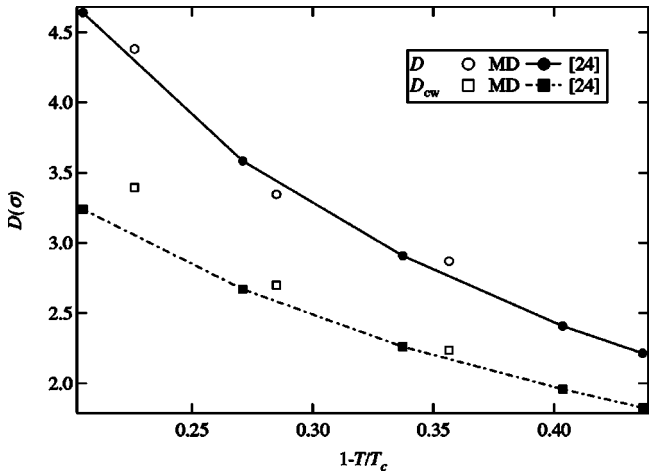

FIG. 2. Interface thickness D and D_{cw}. Open symbols: present work. Lines and closed symbols: experiments [24].

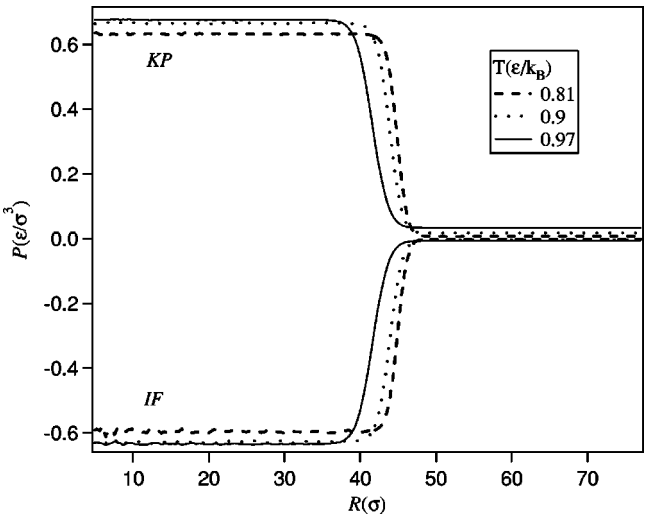

FIG. 3. Dimensionless pressure profiles in the radial direction for three different temperatures. K=Kinetic component, IF =Internal Forces component.

[25] conducted on smaller clusters ($5<R_e<10$) showing that, within the error limit, the surface tension seems to be curvature independent. The normal pressure profile is evaluated using the algorithm of Thomson *et al.* [22] to solve the spherical extension of Irving-Kirkwood's formula:

$$p_N(r) = k_B T \rho(r) - \frac{1}{4\pi r^2} \sum_k f_k \tag{13}$$

where f_k is the normal component of forces acting across a control surface between a pair of atoms. The first term in the right-hand side of Eq. (13) represents the kinetic contribution (*KP*) to the total pressure while the second is the contribution due to internal forces (*IF*). In Fig. 3 the two components *IF* and *KP* are shown for the three temperatures examined. The pressure difference Δp in Eq. (12) is not obtained directly from Eq. (13), but by adding the asymptotic values of *IF* and *KP* (Fig. 3) inside liquid and vapor where the required relative standard deviation was less than 0.5% in order to minimize the error due to the compensation of the two terms in the right-hand side of Eq. (13).

Table II summarizes the values calculated for the densities ρ_l and ρ_v, surface tension γ, pressures p_v and p_l, and the equimolar dividing radius R_e for the three cases studied. The corresponding experimental values of ρ_l, ρ_v, and γ for argon are also reported for comparison. The MD simulation results predict well the experimental values except for the surface tension of the case $T(\varepsilon/k_B)=0.97$ (the difference is around 10%). This is probably due to a nonperfect thermal equilibrium despite the long-time calculation required.

C. Droplet oscillation

In order to study the oscillation behavior of the droplet after the thermal equilibrium was reached, an impulsively imposed linear velocity field $\nu_\alpha = 2\sqrt{\varepsilon/m}\alpha$ $(\alpha = y, z)$, is applied to each molecule of coordinates x, y, and z inside the liquid region to obtain an initially ellipsoid shape. Subsequently, the drop is allowed to oscillate freely. The temperature increase due to this energy input into the system can be considered negligible (less than 1%) so that it will be assumed that the thermodynamic parameters are the same as that of the equilibrated droplet.

Figure 4 depicts the atomic positions inside the liquid region during the oscillation in four different time steps for the case $T(\varepsilon/k_B)=0.9$. The first picture reports the maximum deformation of the droplet along the x direction. This instant will be considered as the initial stage of the temporal evolution. The maximum deformation along the y-z direction is very small and difficult to capture (third picture). Finally, a spherical shape is reached (fourth picture) with no other visible oscillations.

TABLE II. MD calculation and argon experimental values [14]. Comparison for liquid/vapor densities ρ_l, ρ_v and pressures P_l. P_v; equimolar radius R_e; and surface tension γ.

$T(\varepsilon/k_B)$	$\rho_v(\sigma^{-3})$	$\rho_l(\sigma^{-3})$	$\gamma(\varepsilon/\sigma^2)$	$P_l(\varepsilon/\sigma^{-3})$	$P_v(\varepsilon/\sigma^{-3})$	$R_e(\sigma)$	
0.81	0.008	0.794	0.70	—	—	—	Experimental [14]
0.81	0.010	0.781	0.67	3.73*e*−2	7.5*e*−3	44.85	Present work
0.9	0.017	0.749	0.52	—	—	—	Experimental [14]
0.9	0.020	0.737	0.51	3.95*e*−2	1.6*e*−2	43.87	Present work
0.97	0.030	0.709	0.39	—	—	—	Experimental [14]
0.97	0.033	0.698	0.36	4.38*e*−2	2.68*e*−2	41.89	Present work

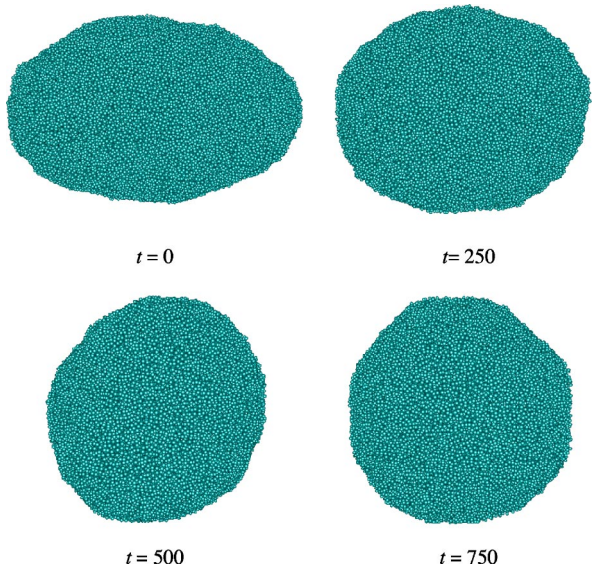

FIG. 4. Particle location inside the liquid region at four different time steps for the case $T(\varepsilon/k_B)=0.9$, time in $\sigma\sqrt{m/\varepsilon}$ units.

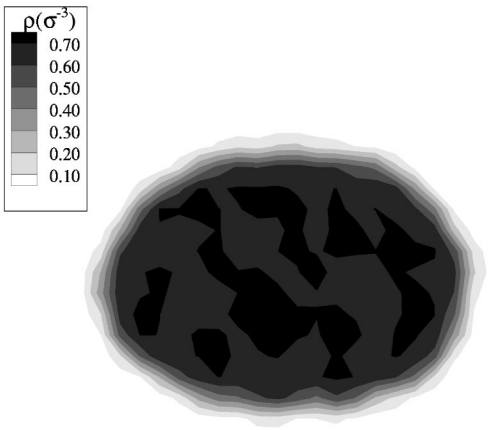

FIG. 5. Density field in a cross section in the middle plane during deformation.

To evaluate the magnitude of the droplet deformation, the computational domain is divided into $30\times30\times30$ bins, and a first-order interpolation scheme is used to convert the Lagrangian description of the atom simulation to an Eulerian-type iso-surface of density. Subsequently, a least-squares interpolation was used to fit the particles inside regions with a density $\rho(R_e)\pm0.01\rho(R_e)$, (i.e., within a small range of density corresponding to that of the equimolar radius in the equilibrated configuration), onto an ellipsoid, in order to evaluate the three axes a, b, and c of the deformed droplet. This procedure gave the same qualitative results obtained by evaluating the gyration radius along the three axis defined as: $R_\alpha=1/N\Sigma_{i=1}^{N}\alpha_i^2$, where $\alpha=x,y,z$.

Figure 5 shows a typical density field in a cross section in the middle plane during the deformation. Due to the interpolation technique and the large number of atoms in each cell, a good spatial definition is achieved without time averaging.

The time behavior of a/b, is depicted in Fig. 6 for the case $T(\varepsilon/k_B)=0.81$. As observed before, only one oscillation period can be seen; further oscillations are damped by viscosity and become indistinguishable from the noise due to capillary waves. Moreover, when the oscillation amplitude is comparable with the amplitude of capillary waves, the assumption of an ellipsoid shape is not anymore realistic.

During the first deformation transient (negative time with respect to the curve reported in Fig. 6), the mean temperature of the system exhibits also a harmonic damped behavior (Fig. 7). The period and the dumping constant are small compared to those reported below for the droplet oscillation. This fluctuation is probably caused by the externally imposed velocity field that is perturbing the initially equilibrated configuration decreasing the distances among the atoms. This event is leading to a harmonic damped oscillation of the potential and kinetic energy (the total energy of the system is constant), hence the temperature that is persisting until the droplet reaches its maximum deformation. The period t_T and the damping constant τ of the temperature oscillation are calculated by fitting the MD results with the function

$$T(t) = T_0 \sin\left(\frac{2\pi}{t_T}t + \phi\right)e^{-t/\tau} + T_{av} \tag{14}$$

where T_0 is the initial oscillation temperature amplitude, T_{av} the average temperature, and ϕ the phase. Results are reported in the last two lines of Table I for all cases studied. It appears that both parameters are practically linear functions of the temperature.

For the present study, the Reynolds number, which is a measure of the relative effect of viscosity compared to inertia, is $2.17<\mathrm{Re}<2.52$. The values of ν were set equal to the experimental argon values [14]. If the nonlinearities due to oscillation amplitude and viscosity are small, the second mode oscillation amplitude can be approximated [6,26] as follows:

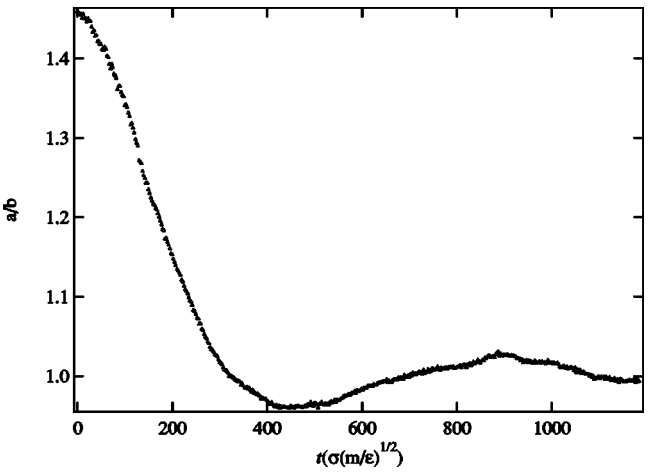

FIG. 6. Ratio between the two interpolated ellipsoid axes during the droplet oscillation for the case $T(\varepsilon/k_B)=0.8$.

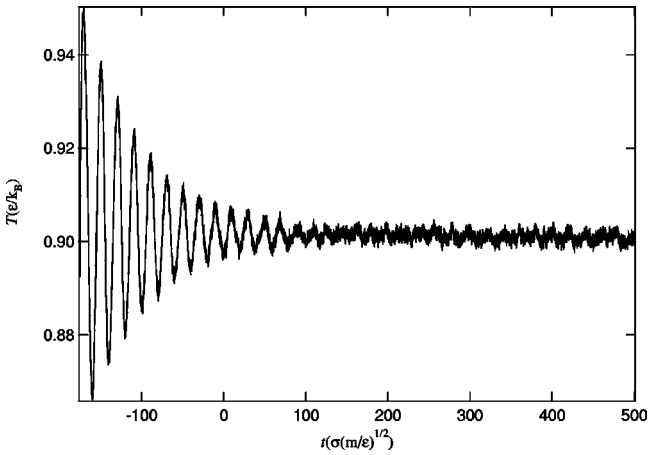

FIG. 7. Time behavior of the system temperature during the deformation transient for the case $T(\varepsilon/k_B)=0.9$.

$$\xi(t) = A\sin\left\{\omega_2\left[\sqrt{1-\left(\frac{b_2}{\omega_2}\right)^2}+\alpha A^2\right]t+\varphi\right\}+\beta A^2 \tag{15}$$

where α accounts for the oscillation amplitude influence on the frequency, β for the asymmetry of the oscillation between the prolate and the oblate deformation, and φ for the phase. The amplitude damping is evaluated as

$$A(t) = A_0\exp(-b_2 t). \tag{16}$$

The oscillation amplitudes of all cases were fitted with Eqs. (15) and (16) using as fitting parameters A_0, α, β, φ, b_2, and ω_2 (Fig. 8). The initial droplet deformations $A_0=a/R-1$ achieved after the compression phase are 0.29, 0.34, and 0.34 for the temperatures $T(\varepsilon/k_B)=0.81$, 0.9, and 0.97, respectively.

The resulting values of ω_2, b_2, and α are reported in Table III in dimensionless units. The values of ω_2 obtained from Eq. (1) are also reported for comparison. The asymptotic frequencies (ω_2) obtained by Eqs. (15) and (16) are quite close to that predicted by Rayleigh's linear analysis [the largest difference is approximately 8% for $T(\varepsilon/k_B)=0.9$]. The parameter α is ranging from -0.32 to -2.6. The latter value, corresponding to the case $T(\varepsilon/k_B)=0.97$, is quite large and denotes a marked decrease in the oscillation frequency with the oscillation amplitude (Becker, Hilla, and Kowalewski [6] obtained with continuum theory $-0.6<\alpha<-0.9$ for a droplet that had a maximum initial deformation $A=0.65$ and $\mathrm{Re}\gg 1$) so that the observed oscillation is quite close to that of the case $T(\varepsilon/k_B)=0.9$. It has to be stressed

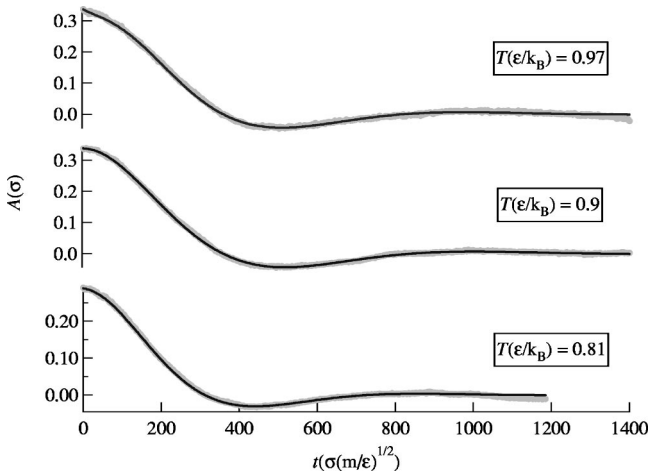

FIG. 8. Oscillation amplitude MD and fit with Eqs. (15) and (16).

that the fitting procedure is not entirely accurate due to the fact that only one oscillation is visible before the droplet becomes practically a sphere and for the higher temperature case the amplitude fluctuations due to capillary waves are large. The values obtained for β are in the same range with those found by Becker *et al.* [6].

A direct comparison of the damping constant b_2 with the corresponding value of Eq. (3) cannot be made because this equation uses the shear viscosity, neglecting the effects of the bulk viscosity. However, it is of interest to report that, possibly due to this viscosity inconsistency, the computed values for b_2 (reported in Table III) are approximately 30% smaller than the b_2 values obtained from Eq. (3). This underlines the importance of bulk viscosity contribution in a compression and volume change process like the one we are studying here.

IV. CONCLUSIONS

The oscillatory behavior and related thermophysical properties of nanodroplets were studied using molecular dynamics simulations. Using a proper cutoff distance it was possible to obtain the experimental values of density and surface tension for argon with a good approximation. The surface thickness due to capillary waves based on continuum theory was quantified to be around 86% of the total surface thickness evaluated via MD. A linear interpolation scheme was used to obtain a Lagrangian formulation of the system in order to calculate the oscillation amplitude of the droplet. Although due to the viscosity effects only one oscillation

TABLE III. Fitting parameters of Eqs. (15) and (16) describing the droplet oscillation behavior for the three studied temperatures.

$T(\varepsilon/k_B)$	$\omega_2\,(\sigma\sqrt{m/\varepsilon})^{-1}$ MD	$\omega_2\,(\sigma\sqrt{m/\varepsilon})^{-1}$ Eq. (1)	α	β	$b_2\,(\sigma\sqrt{m/\varepsilon})^{-1}$
0.81	0.0090	0.0088	−0.91	0.32	0.0050
0.9	0.0075	0.0082	−0.32	0.32	0.0039
0.97	0.0077	0.0074	−2.72	0.29	0.0040

period is visible, typical phenomena that are described in previous works both experimental and numerical/theoretical based on continuum theory, were observed. The frequency of the oscillation decreases for the finite oscillation amplitude and the prolate phase lasts longer than the oblate. The values obtained for the asymptotic frequencies are in good agreement with that of Rayleigh's linear theory. In all it was found that the continuum analysis can predict reasonably well the oscillation behavior of nanodroplets, although quantitative differences exist.

ACKNOWLEDGMENT

This work was supported by the Forschungskommission of ETH.

[1] L. Rayleigh, Proc. R. Soc. London **29**, 71 (1879).
[2] H. Lamb, *Hydrodynamics* (Dover, New York, 1932).
[3] S. Chandrasekhar, Proc. London Math. Soc. **9**, 141 (1959).
[4] A. Prosperetti, J. Fluid Mech. **100**, 333 (1980).
[5] J.A. Tsamopoulos and R.A. Brown, J. Fluid Mech. **127**, 519 (1983).
[6] E. Becker, W.J. Hiller, and T.A. Kowalewski, J. Fluid Mech. **231**, 189 (1991).
[7] O.A. Basaran, J. Fluid Mech. **241**, 169 (1992).
[8] F. Mashayek and N. Ashgriz, Phys. Fluids **10**, 1071 (1998).
[9] C. Pozrikidis, Comput. Fluids **30**, 417 (2001).
[10] E. Trinh and T.G. Wang, J. Fluid Mech. **122**, 315 (1982).
[11] T.G. Wang, A.V. Anilkumar, C.P. Lee, and K.C. Lin, J. Fluid Mech. **276**, 389 (1994).
[12] H. Azuma and S. Yoshihara, J. Fluid Mech. **393**, 309 (1999).
[13] A. Trokhymchuk and J. Alejandre, J. Chem. Phys. **111**, 8510 (1999).
[14] http://webbook.nist.gov
[15] M.P. Allen and D.J. Tildesley, *Computer Simulation of Liquids* (Clarendon, Oxford, 1987).
[16] S. Plimpton, J. Comput. Phys. **117**, 1 (1995).
[17] S.W. Sides, G.S. Grest, and M.D. Lacasse, Phys. Rev. E **60**, 6708 (1999).
[18] S. Toxvaerd and J. Stecki, J. Chem. Phys. **115**, 1928 (2001).
[19] L.S. Bartell, Surf. Sci. **397**, 217 (1998).
[20] L.S. Bartell, J. Mol. Struct. **445**, 59 (1998).
[21] M.J.P. Nijmeijer, C. Bruin, A.B. Vanwoerkom, A.F. Bakker, and J.M.J. Vanleeuwen, J. Chem. Phys. **96**, 565 (1992).
[22] S.M. Thompson, K.E. Gubbins, J. Walton, R.A.R. Chantry, and J.S. Rowlinson, J. Chem. Phys. **81**, 530 (1984).
[23] J. Lekner and J.R. Henderson, Physica A **94**, 545 (1978).
[24] D. Beaglehole, Physica B & C **100**, 163 (1980).
[25] H. El Bardouni, M. Mareschal, R. Lovett, and M. Baus, J. Chem. Phys. **113**, 9804 (2000).
[26] B. Stuckrad, W.J. Hiller, and T.A. Kowalewski, Exp. Fluids **15**, 332 (1993).